THE JOURNAL OF PHYSICAL CHEMISTRY C

Article

Cite This: J. Phys. Chem. C 2019, 123, 26870−26876

pubs.acs.org/JPCC

Intrinsic Controllable Magnetism of Graphene Grown on Fe

Jeongmin Hong,*[,†,‡] Yooseok Kim,[§] Jinghua Liang,[∥,⊥] Hong Chen,[#] Chong-Yun Park,[§] Hongxin Yang,[∥,⊥] Elton J. G. Santos,[▽,○] Jeffrey Bokor,[‡] Chan-Cuk Hwang,*[,◆] and Long You*[,†]

[†]School of Optical and Electronic Information, Huazhong University of Science and Technology, Wuhan 430074, China

[‡]EECS, UC Berkeley, Berkeley, California 94720, United States

[§]Department of Physics, Sungkyunkwan University, Suwon 16419, Korea

[∥]Ningbo Institute of Materials Technology and Engineering, Chinese Academy of Sciences, Ningbo 315301, China

[⊥]Center of Materials Science and Optoelectronics Engineering, University of Chinese Academy of Sciences, Beijing 100049, China

[#]School of Materials Science and Energy Engineering, Foshan University, Foshan, Guangdong 528000, China

[▽]School of Mathematics and Physics, Queen's University, Belfast BT7 1NN, United Kingdom

[○]Department of Chemical Engineering, Stanford University, Stanford, California 94305, United States

[◆]Beamline Division, Pohang Accelerator Laboratory (PAL), POSTECH, Pohang 37673, Korea

Supporting Information

ABSTRACT: Novel functional materials that use both the spin and charge of an electron offer many exciting opportunities to create new information processing and storage devices with ultralow power consumption. The recent discovery of magnetism in atomically thin-layered materials could boost research in the field of light element materials such as van der Waals magnetic nanostructures. Here, we report intrinsic magnetization in large-area graphene grown on Fe(100) foil structures. The optimal growth mechanisms provide high-quality graphene samples with controllable magnetic properties, such as thickness-dependent magnetization. Using first-principles calculations, we investigated several possible scenarios for controlling the magnetic properties. Moreover, the independent magnetic structures induced in graphene were identified through field-applied magnetic force microscopy (FA-MFM) followed by vibrating sample magnetometry (VSM). Our results open a new avenue for controlling the magnetic properties of graphene structures by mediating surface growth on regular magnets for applications in large-scale spintronics.

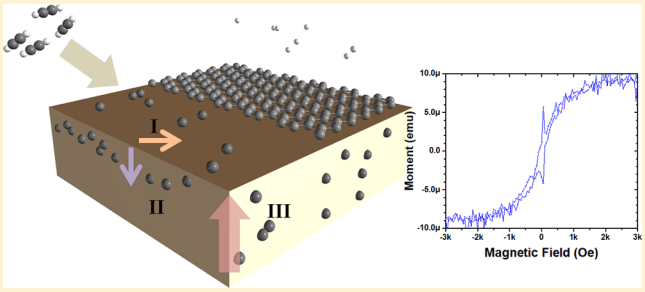

INTRODUCTION

Computing using magnetic chips can reduce power consumption to one millionth of the amount used by today's transistors.[1−3] Such materials could be designed with multifunctional characteristics, including controllable magnetic properties and superior electric, photonic, thermal, and other physical properties. The quantum phenomena in magnetic graphene include quantum spin Hall effects, long spin-relaxation times, a long electronic mean free path, and ballistic spin transport at room temperature with the potential to tune spin−orbit interactions.[4−8] Moreover, the spin-diffusion length of graphene has been reported to be 1−2 μm at room temperature.[7] The recently developed van der Waals 2D magnetism indicates the need to study magnetic graphene.[9] Multifunctional carbon-based 2D nanomaterials perform information processing using spin states at the Fermi level. The magnetic ordering and induced ferromagnetism of carbon-based nanostructures have long been investigated in a variety of ways.[10−19] However, due to the lack of controllability and the nonuniformity of synthesized structures, such magnetic carbon properties are challenging to apply in practical spintronic devices. For this reason, large-area magnetic graphene is required for further practical applications.

MATERIALS AND METHODS

Synthesis of Graphene. Graphene was grown on 100 μm thick Fe foil (Nilaco, 99.99% purity) in a hot furnace consisting of a 50 mm quartz tube. Fe foil was first placed in the center of a horizontal quartz tube. After H_2 (100 standard cubic centimeters per unit, sccm) and Ar (200 sccm) were introduced as the carrier gases and the furnace temperature reached 800 K, Fe foil was preannealed at 800 K (the Fe phase will change above 850 K) for 30 min to remove the native Fe oxide layer and enlarge the Fe grains in the H_2 and Ar

Received: June 20, 2019
Revised: October 13, 2019
Published: October 14, 2019

DOI: 10.1021/acs.jpcc.9b05886
J. Phys. Chem. C 2019, 123, 26870−26876

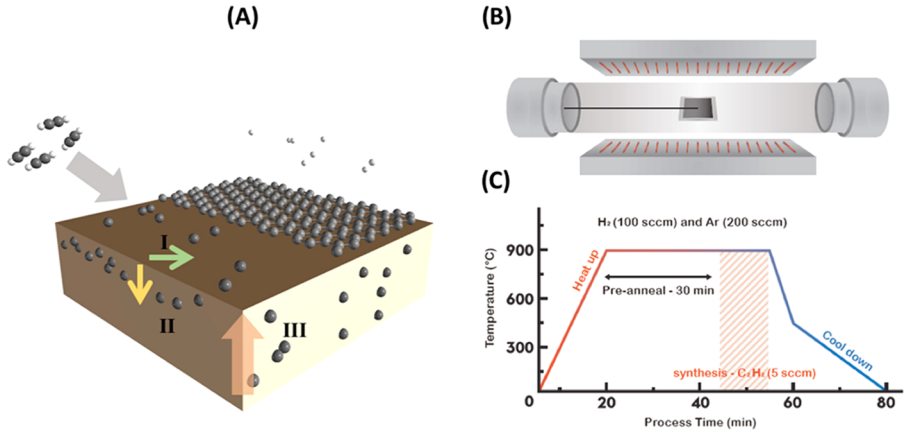

Figure 1. Synthesis mechanisms of graphene on Fe: (A) Schematic of the synthesis scenarios of magnetic graphene. (B) Schematic illustration of graphene growth in a chemical vapor deposition (CVD) system. (C) Optimal parameters for the synthesis of graphene on Fe using a CVD system.

atmosphere. Fe changes its phase above 800 K. Then, C_2H_2 (5 sccm) was introduced, with the process pressure set to 500 mTorr during growth. After C_2H_2 was introduced, the furnace was cooled to room temperature with H_2 and Ar.

Raman Spectroscopy. Raman spectroscopy (Reinshaw, RM1000-Invia) with a laser excitation wavelength of 514 nm (2.41 eV), a notch filter cutoff frequency of 50 nm^{-1}, and a focus spot size of 5 μm was used to measure the crystallinity and the number of layers in the graphene films. Few-layer graphene was synthesized with times of 1, 3, 6, and 9 min, and a very strong 2D peak at ~2700 cm^{-1} and a G peak at ~1580 cm^{-1} appeared in each Raman spectrum. Additionally, the D peak at ~1350 cm^{-1} was observed.

Scanning and Transmission Electron Microscopy (SEM and TEM). To inspect the exact thickness of the synthesized graphene, high-resolution transmission electron microscopy (HR-TEM, JEOL, JEM-2100F) measurements were performed to estimate the number of layers of graphene.

Atomic Force Microscopy/Magnetic Force Microscopy. Scanning probe microscopy (SPM) was performed in noncontact mode using a Bruker-Nano AFM system. The MFM measurements were conducted in a dynamic lift mode with a lift distance of 30 nm. The dynamics were measured in the presence of a magnetic field by sweeping the field range.

Vibrating Sample Magnetometry (VSM). The conventional volume averaging magnetometry measurements were performed using a VSM 7400 from Lake Shore Cryotronics Inc. with a 3.1−T electromagnet. The sample was mounted on a quartz holder. The magnetic moment was measured and averaged. The in-plane crystalline anisotropy is shown in Figure S5. In this type of crystal structure, the domain is randomly oriented and the sizes of the domain structures are very large (more than a micron).

First-Principles van der Waals Ab Initio Calculations. The calculations reported herein are based on ab initio density function theory using the SIESTA method[20] and the VASP code.[21,22] The generalized gradient approximation[23] along with the DRSLL[24] functional was used in both methods, together with a double-ζ polarized basis set in SIESTA and a well-converged plane-wave cutoff of 500 eV in VASP. The projected augmented wave method (PAW)[25,26] was used for the latter and the norm-conserving (NC) Troullier−Martins pseudopotentials[27−34] were used for the former to describe the bonding environments for Fe and C. The shape of the NAOs was automatically determined by the algorithms described in S1. The cutoff radii of the different orbitals were obtained using an energy shift of 50 meV, which proved to be sufficiently accurate to describe the geometries and energetics. Atomic coordinates were allowed to relax until the forces on the ions were less than 0.01 eV/Å under the conjugate gradient algorithm. To model the system studied in the experiments, we created large supercells containing up to 1382 atoms to simulate the interface between the multilayer graphene and Fe surfaces. We initially used three different facets, such as (111), (110), and (100), to represent the Fe substrates. We used all three at the monolayer graphene limit and the Fe(100) facet for multilayer graphene, as a high concentration of these facets was found in the Fe foil. To avoid any interactions between supercells in the nonperiodic direction, 20 Å was used in all calculations. In addition, a cutoff energy of 120 R_y was used to resolve the real-space grid for calculating the Hartree and exchange−correlation contribution to the total energy. The Brillouin zone was sampled with a 10 × 10 × 1 grid under the Monkhorst−Pack scheme[35] to perform relaxations with and without van der Waals interactions. A few geometries required a finer grid of 15 × 15 × 1 to fully relax the atomic forces. Energetics were calculated using converged 25 × 25 × 1 k-sampling. In addition, we used a Fermi−Dirac distribution with an electronic temperature of k_BT = 21 meV to resolve the electronic structure.

RESULTS AND DISCUSSION

Graphene was grown on 100 μm thick Fe foils in a hot furnace. By varying the deposition parameters, such as the time and temperature, the thickness of the graphene was systematically controlled. Figure 1 shows a schematic of the synthesis (A) and experimental setup (B) and a graph of the synthesis conditions (C). As shown in Figure 1A, the well-known growth mechanisms are described, including surface adsorption, diffusion, and precipitation.[20] Two mechanisms are considered to govern the growth of graphene on typical catalysts, such as Cu and Ni.[21,22] The extremely low carbon solubility of Cu leads to the self-limited growth of graphene via the simple thermal decomposition of hydrocarbons on the Cu surface, as shown in scenario (I). In contrast, the high carbon solubility of Ni causes carbon to dissolve into the bulk and graphene subsequently grows through the surface segregation of carbon upon cooling from a metastable carbon-metal solid solution (II). The formation of graphene on Fe simultaneously follows

DOI: 10.1021/acs.jpcc.9b05886
J. Phys. Chem. C 2019, 123, 26870−26876

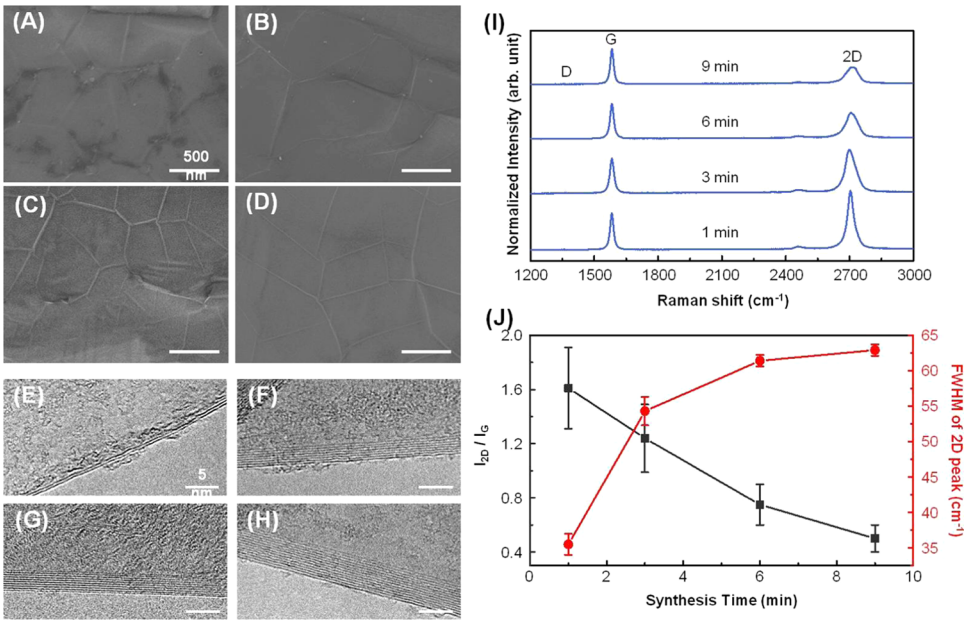

Figure 2. SEM micrographs of graphene with increasing synthesis times of (A) 1 min, (B) 3 min, (C) 6 min, and (D) 9 min. The TEM images during the synthesis: (E) 1 min (2 layers), (F) 3 min (8 layers), (G) 6 min (10 layers), and (H) 9 min (13 layers). The estimated thickness of the sample is as follows: 1 min of synthesis time for 2 layers, 3 min for 8 layers, 6 min for 10 layers, and 9 min for 13 layers. (I) The Raman spectra for the increasing synthesis time: 0, 1, 3, 6, and 9 min. (J) Ratio of the 2D and G peaks and the FWHM of the 2D peaks. The estimation is based on the Raman spectra and TEM images.

both mechanisms I and II. The experimental results show that graphene can also be synthesized using the intrinsic carbon contained inside the iron substrates (III), which could be a unique mechanism for growing magnetic carbon.[23] The detailed synthesis conditions and experimental parameters are shown in the Materials and Methods section. It is very challenging to grow bulk graphene on Fe substrates. We developed a combined synthesis technique to achieve high-quality graphene on Fe using an acetylene (C_2H_2) feedstock, even if the Fe drastically dissolved carbon. Layer-controlled graphene films were successfully synthesized on the substrate in selective growth windows with a finely tuned C_2H_2, Ar, and H_2 gas ratio and growth time, which make it possible to prove thickness-dependent magnetization, as shown in Figure 1C.

Figure 1B shows a schematic of the CVD systems with the graphene sample for the optimal synthesis. First, 30 min of preannealing and plasma sputtering was performed to clean the surface, as shown in Figure 1C. During the preannealing process, Fe-based oxides and impurities on the Fe surface could be removed. By controlling several parameters, such as the temperature range, gas composition, and flow rate, graphene could be synthesized in a controllable layer on Fe by changing the synthesis time, as shown in Figure 1C. The quality of the samples was monitored using high-resolution photoemission spectroscopy (HRPES) at the 10D beamline of the Pohang Accelerator Laboratory (PAL) and commercially available X-ray photoelectron spectroscopy (XPS). Sharp C 1s core-level spectra indicated that the quality of graphene grown on Fe is comparable with that of graphene grown on Ni and Cu.[23,24]

To inspect the quality and exact thickness of the synthesized graphene, scanning electron microscopy (SEM) and high-resolution transmission electron microscopy (HR-TEM) measurements were performed to estimate the number of layers of graphene, as shown in Figure 2A–H. The formation of wrinkles is a well-known phenomenon caused by the difference between thermal expansion coefficients of Fe and graphene, and wrinkles are generated when the foil is rapidly quenched or a growing flake starts to overlap with another nearby flake. Defects and edges are observed in multilayer graphene films. The detailed synthesis, characterization process, and following results are described in the Materials and Methods section. The number of graphene layers can be clearly identified as 2, 8, 10, and 13 based on the interlayer spacing of graphene (0.34 nm). As also shown in our previous reports, the synthesis time can precisely control the number of layers.[23−26]

Raman spectroscopy is a powerful yet relatively specimen-specific measurement used to characterize the crystalline quality and number of graphene layers, as shown in Figure 2I. The D peak depends on the breathing mode of the 6-fold aromatic ring (sp^3), is independent of the number of graphene layers and is activated by disorder. The G peak is due to the doubly degenerate zone in the center E_{2g} mode. Since the generation of the 2D peak is a process allowing symmetry, the band of the second-order Raman process appears with no relation to any defect or disorder. The 2D peak even provides a count of the number of graphene sheets in a specimen. Other criteria used to measure the number of graphene layers are the full width at half maximum (FWHM) and the position of the 2D peak. Additionally, the intensity ratio of the 2D to G peaks (I_{2D}/I_G) is dependent on the number of layers. As shown in Figure 2J, the ratio of I_{2D}/I_G was approximately 1.61, 1.24, 0.75, and 0.55, for 1, 3, 6, and 9 min of synthesis time, respectively. In the bottom spectrum in Figure 2J, the intensity ratio is 1.61 and the peak position of the symmetric 2D band is 2700 cm^{-1} with a FWHM of 35.5 cm^{-1}, which is in accordance with the parameters of bilayer graphene.

Raman spectra are sometimes ambiguous in estimating the number of layers of graphene, especially few-layer graphene.

DOI: 10.1021/acs.jpcc.9b05886
J. Phys. Chem. C 2019, 123, 26870−26876

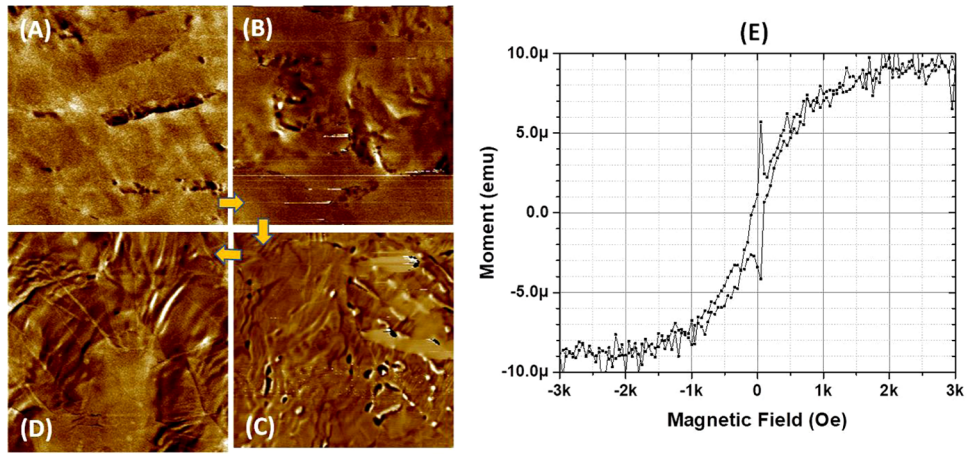

Figure 3. Magnetic imaging characteristics. (A) Magnetic force microscopy (MFM) image of the magnetic domains of graphene on Fe(100) foil, which shows the different domain structures of Fe(100). The MFM images show the increasing thicknesses: (A) 2, (B) 8, (C) 10, and (D) 13. The brighter and darker regions represent the changes in the magnetic phase. The images are $3 \times 3\ \mu m^2$. (E) m−H loop of graphene after transfer to the SiO_2 substrate. The presence of mixed antiferromagnetic (AFM) and ferromagnetic (FM) behaviors was observed.

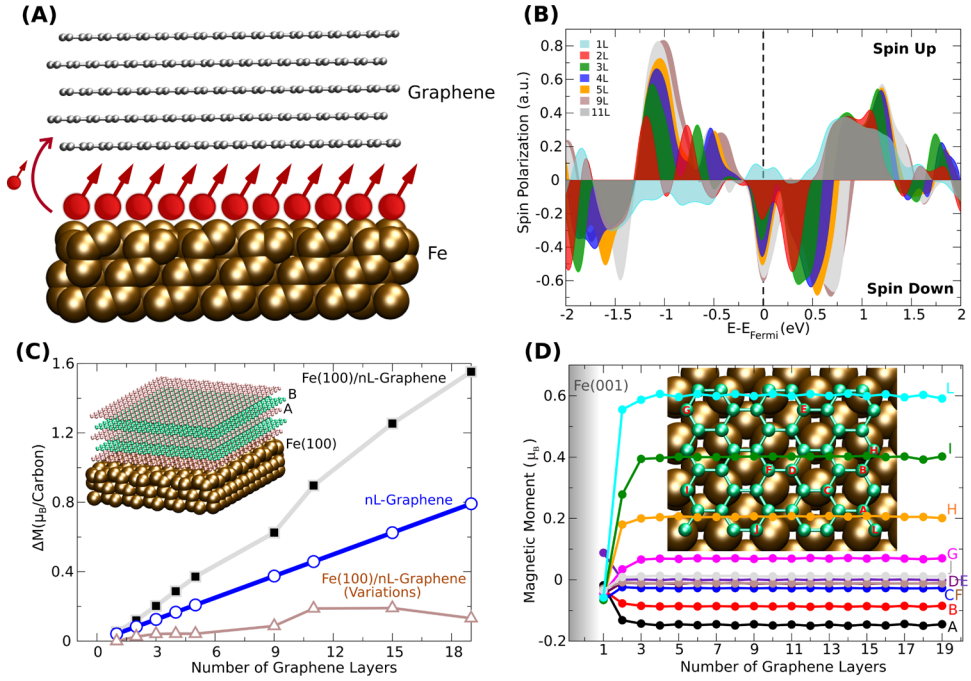

Figure 4. First-principles simulations of graphene on Fe(100). (A) Schematic of the spin transfer from Fe to multilayer graphene. The polarized spin states at the interface induce a finite spin moment in the carbon states. To avoid spurious artifacts from the difference in the lattice mismatch between graphene and Fe(100), the graphene layers are modeled in terms of nanoribbons with H-saturated edges, as shown in the inset in (D). A finite spin moment is observed at the zigzag edges, which can be separated from the bulk carbons where no spin moment is initially present before making the interface with Fe. (B) Spin polarization ξ versus energy for different numbers of graphene layers on Fe(100). ξ is defined in terms of $\xi = n^{up} - n^{down}/n^{up} + n^{down}$, where n^{down} and n^{up} are the densities of states of the spin-up and spin-down states, respectively. The spin polarizations for different numbers of layers are highlighted in different colors. The Fermi level is set to zero in all curves. Interestingly, the first layer close to the Fe surface is magnetically coupled to Fe in an opposite way than the others. That is, if Fe is ferromagnetic, the first graphene layer in contact with Fe is antiferromagnetic, and vice versa. (C) Magnetization ΔM (Bohr magneton per carbon) of the nanoribbons as a function of the number of graphene layers on Fe(100). The value of ΔM is defined through $\Delta M = M_{total} - m_{graphene}$, where $m_{graphene}$ is the net spin moment present at the graphene ribbons, and M_{total} is the magnetization of the system. Gray, blue and faint brown curves correspond, respectively, to Fe(100)/nL-graphene systems, isolated nL-graphene layers and the variation in the magnetization per layer for Fe(100)/nL-graphene relative to the immediate previous layer number. The inset shows a molecular schematic of the graphene layers on the Fe(100) surface with AB stacking. The magnetic moment at the carbons linearly increases with the number of sheets (blue curve) due to the finite moment at each individual layer but is substantially enhanced when the nanoribbons are combined with Fe(100). This indicates that the Fe surface has a clear effect on the magnetization of defects/edges once the interface is created. This result is in sound agreement with the experiments shown in Figure 2. (D) Local magnetic moment (Bohr per carbon) versus the number of graphene layers at some of the carbon atoms on the Fe(100) substrate. Carbon atoms near defects or imperfections (e.g., vacancies) tend to be easily polarized as the number of layers increases but suffer strong reduction in thinner systems due to competition with charge transfer.

DOI: 10.1021/acs.jpcc.9b05886
J. Phys. Chem. C 2019, 123, 26870−26876

The HR-TEM results agreed well with the Raman results and clearly showed that the number of graphene layers increased with increasing synthesis time. As a result, Raman spectra together with HR-TEM and SEM images confirm the different numbers of layers and defects in the samples.

Our study of field-applied (FA)-MFM with X-ray magnetic circular dichroism (XMCD) provides strong confirmation that this technique can be used to probe the magnetic domain structure of materials in local regions. The FA-MFM image shown in Figure 3A indicates similar domain patterns for the graphene grown on Fe foil, which are very different from those of bcc Fe(100) bulk structures. The domain structures of the Fe crystal changed from a randomly oriented large domain to a smaller domain pattern after the synthesis of graphene. The magnetic stripe domain structures could be an indication of the dominant crystalline structure after the synthesis process. As shown in Figure 3A−D, small domain structures can be observed in the graphene on the Fe sample. The orientation of the magnetization in the plane is shown in the SI. The domain structures change as the layer number increases. The results confirm that controllable magnetic properties are observed in the domain patterns. The image contains topographical information and magnetic phases together because of the nonuniform nature of large-area graphene. However, FA-MFM can observe the phase change from a fully saturated magnet underneath. Thus, the systems probe the magnetic properties of carbon, which indicate simultaneous independent domain formations from the Fe substrate.

After we transfer the sample to nonmagnetic substrates, we can still observe small magnetization, which confirms that the effects are intrinsic. Using a stamping method, we selectively transferred graphene from Fe to SiO_2 substrates. Then, we carefully checked the X-ray spectra using synchrotron radiation at ALS. The results indicated that the aligned carbon edges and defects play a critical role in increasing the magnetic moment of graphene. As shown in Figure 3E, m−H loops indicate the presence of ferromagnetism (FM) and antiferromagnetism (AFM), which have already been previously reported.[13,15−17] The XMCD at the 1s C-edge confirms magnetic moment of carbon as shown in the SI. Another important note is that light element magnetism usually comes from proximity effects resulting from hybridization between the transition metal and graphene. This is partly true, but the contribution could be smaller than that in the case of Fe foil because of the lattice mismatching. If we manipulate the systematic controllability, spin devices can be created.

We performed a theoretical validation of the experimental results. The model structure of graphene grown on Fe is shown in Figure 4A, and the spin-polarized interface is highlighted. Once graphene is formed on the Fe surface, the proximity effect polarizes the carbon states near the Fermi level, and only one spin channel is observed to be pinned at the Fermi level (Figure 4B). The Fe surface is the main source of spin-polarized carriers because the number of states per eV for one spin channel, e.g., spin down, is substantially higher than that for spin up (Figure S3A in the Supporting Information). We also observed that the number of polarized states in graphene increases with the layer thickness, and a transition from one spin state to another occurs as we cross from monolayer (1L) to bilayer (2L), that is, from spin up to spin down. The strong interactions between the nearest graphene layer and the Fe substrate make the exchange interactions favorable for this antiferromagnetic coupling by 15.4 meV (Figure S3B). Figure 4C shows that the magnetization in the first layers is also smaller than that in the thicker systems, which can also be observed locally at each individual C atom in each layer (Figure 1D). This difference indicates an enhancement in the magnetic properties with the growth process. However, the enhancement saturates with approximately 15 carbon sheets on Fe, and the increment of the magnetic moments begins decreasing thereafter. One of the main reasons for this thickness dependence can be observed in the amount of charge transfer from the Fe substrate to graphene (Figure S3C), which is substantially larger for the layers near the Fe and exponentially decays throughout the system. The amount of charge transfer is closely related to the position of the Fermi level at the interface, which shows an oscillatory-like behavior with the layer thickness (Figure S3D) until it reaches a constant value at approximately 9 layers. Then, as more layers are deposited, the magnetic moment tends to decay. Four possible cases were considered for the observed ferromagnetism: defects, layer dependence, proximity effects, and Fe intercalation. Ideal defect and/or edge states in graphene show 0.4 Bohr, which is in close agreement with the experimental magnitudes of ∼0.46 Bohr from magnetization. One of the main reasons for this thickness dependence is the number of defects in graphene, which is substantially larger for the layers near the Fe and exponentially decays throughout the system. Therefore, as more layers are deposited, the magnetization initially increases but decays as thicker carbon is achieved.

From our experimental data with the support of theoretical calculations, layer-controllable graphene samples grown via CVD can provide controllable magnetic properties. The magnetic properties of the graphene samples were measured, and significant changes resulting from defects through the graphene plane were confirmed. Moreover, MFM confirmed the change in the domain patterns, which resulted from the large magnetic moment in pure graphene structures (Table 1).

Table 1. Calculated Bohr Magneton Results for the Possible Factors that Could Generate a Magnetic Moment on Graphene

factors	1st layer	2nd layer
proximity	0.012	0.008
intercalation	0.026	0.021
defects	0.4	0.008 (no defects)

CONCLUSIONS

We have demonstrated a new way to synthesize large-area magnetic graphene with controllable magnetic properties. The estimated magnetization of 0.4 Bohr was observed through calculations performed on a carbon site. The magnetic properties remained after transfer from metal substrates, as shown in the SI. The controllable magnetic properties of a large-area carbon nanostructure would be an excellent building block, such as a spin-polarized electron source at the Fermi level, for future energy-efficient spintronic devices. The results pave a new avenue for light element-based spintronics applications.

ASSOCIATED CONTENT

Supporting Information

The Supporting Information is available free of charge on the ACS Publications website at DOI: 10.1021/acs.jpcc.9b05886.

DOI: 10.1021/acs.jpcc.9b05886
J. Phys. Chem. C 2019, 123, 26870−26876

m−H loop of the bulk materials (Figure S1); X-ray magnetic circular dichroism (XMCD) measurements (Figure S2); magnetic simulations for the Fe-graphene interface (Figure S3); LEED pattern of the Fe foil (Figure S4); Auger electron spectroscopy (Figure S5) (PDF)

AUTHOR INFORMATION

Corresponding Authors

*E-mail: jehong@hust.edu.cn, jehong@berkeley.edu (J.H.).
*E-mail: cchwang@postech.ac.kr (C.-C.H.).
*E-mail: lyou@hust.edu.cn (L.Y.).

ORCID

Jeongmin Hong: 0000-0002-8639-3620
Elton J. G. Santos: 0000-0001-6065-5787
Long You: 0000-0001-5713-194X

Author Contributions

J.H. conceived the idea and designed the experiments. J.H. and C.-C.H. led the experiments (with assistance from Y.K.). J.H., L.Y., J.B., and C.-C.H. contributed to the data analysis and interpretation. J.L., E.J.G.S., and H.Y. performed the calculations. J.H. and C.-C.H. wrote the paper, and all authors provided feedback. The manuscript was written with contributions from all authors. All authors have given approval for the final version of the manuscript.

Notes

The authors declare no competing financial interest.

ACKNOWLEDGMENTS

This work was supported by the National Natural Science Foundation of China under Award number 61674062. J.B. acknowledges financial support from the National Science Foundation (NSF) under Award number 0939514. The work was supported by the U.S. Department of Energy, Office of Basic Energy Sciences, Division of Materials Sciences and Engineering under Contract No. DE-AC02-05CH11231. E.J.G.S. acknowledges the use of computational resources from the UK Materials and Molecular Modeling Hub, which is partially funded by EPSRC (EP/P020194/1; Service (ec019 Cirrus Project) at EPCC (http://www.cirrus.ac.uk) funded by EP/P020267/1; and Department for the Economy (USI 097)) through financial support. C.-C.H. acknowledges the support of the National Research Foundation of Korea (NRF) funded by the Korean government (Ministry of Science and ICT) (No. 2018R1A5A6075964, No. 2017R1A2B2003928, and No. 2017M3A7B4049173).

REFERENCES

(1) Hong, J.; Lambson, B.; Dhuey, S.; Bokor, J. Experimental test of Landauer's principle in single-bit operations on nanomagnetic memory bits. *Sci. Adv.* **2016**, *2*, No. e1501492.
(2) Meindl, J. D.; Davis, J. A. The fundamental limit on binary switching energy for terascale integration. *IEEE J. Solid-State Circuits* **2000**, *35*, 1515−1516.
(3) Wolf, S. A.; Chtchelkanova, A. Y.; Treger, D. M. Spintronics − A retrospective and perspective. *IBM J. Res. Dev.* **2006**, *50*, 101−110.
(4) Kane, C. L.; Mele, E. J. Quantum spin hall effect in graphene. *Phys. Rev. Lett.* **2005**, *95*, No. 226801.
(5) Han, W.; Kawakami, R. K. Spin relaxation in single-layer and bilayer graphene. *Phys. Rev. Lett.* **2011**, *107*, No. 047207.
(6) Bolotin, K. I.; Sikes, K. J.; Jiang, Z.; Klima, M.; Fudenberg, G.; et al. Ultrahigh electron mobility in suspended graphene. *Solid State Commun.* **2008**, *146*, 351−359.
(7) Tombros, N.; Jozsa, C.; Popinciuc, M.; Jonkman, H. T.; van Wees, B. J. Electronic spin transport and spin precession in single layers at room temperature. *Nature* **2007**, *448*, 571−574.
(8) Asmar, M. M.; Ulloa, S. E. Spin-orbit interaction and isotropic electronic transport in graphene. *Phys. Rev. Lett.* **2014**, *112*, No. 136602.
(9) Burch, K. S.; Mandrus, D.; Park, J.-G. Magnetism in two-dimensional van der Waals materials. *Nature* **2018**, *563*, 47−52.
(10) Haddon, R. C. Magnetism of carbon allotropes. *Nature* **1995**, *378*, 249−255.
(11) Yazyev, O. V. Emergence of magnetism in graphene materials and nanostructures. *Rep. Prog. Phys.* **2010**, *73*, No. 056501.
(12) Son, Y.-W.; Cohen, M. L.; Louie, S. G. Half-metallic graphene nanoribbons. *Nature* **2006**, *444*, 347.
(13) Hong, J.; Bekyarova, E.; de Heer, W. A.; Khizreov, S.; Haddon, R. C. Chemically engineered graphene-based 2D organic molecular magnet. *ACS Nano* **2013**, *7*, 10011−10022.
(14) Sepioni, M.; Nair, R. R.; Rablen, S.; Narayanan, J.; Tuna, F.; et al. Limits on intrinsic magnetism in graphene. *Phys. Rev. Lett.* **2010**, *105*, No. 207205.
(15) Hong, J.; Bekyarova, E.; de Heer, W. A.; Haddon, R. C.; Khizroev, S.; et al. Room-temperature magnetic ordering in functionalized graphene. *Sci. Rep.* **2012**, *2*, No. 624.
(16) Hong, J.; Niyogi, S.; Bekyarova, E.; Itkis, M. E.; Ramesh, P.; Amos, N.; Litvinov, D.; Berger, C.; de Heer, W. A.; Khizroev, S.; Haddon, R. C. Effect of nitrophenyl functionalization on the magnetic properties of epitaxial graphene. *Small* **2011**, *7*, 1175−1180.
(17) Niyogi, S.; Bekyarova, E.; Hong, J.; Khizroev, S.; Berger, C.; de Heer, W. A.; Haddon, R. C. Covalent chemistry for graphene electronics. *J. Phys. Chem. Lett.* **2011**, *2*, 2487−2498.
(18) Vinogradov, N. A.; Zakharov, A. A.; Kocevski, V.; Rusz, J.; Simonov, K. A.; et al. Formation and structure of graphene waves on Fe (110). *Phys. Rev. Lett.* **2012**, *109*, No. 026101.
(19) Liu, W. Q.; Wang, W. Y.; Wang, J. J.; Wang, F. Q.; Lu, C.; et al. Atomic-scale interfacial magnetism in Fe/Graphene heterojunction. *Sci. Rep.* **2015**, *5*, No. 11911.
(20) José, M. S.; et al. The SIESTA method for ab initio order- N materials simulation. *J. Phys.: Condens. Matter* **2002**, *14*, 2745−2779.
(21) Kresse, G.; Hafner, J. Ab initio molecular dynamics for open-shell transition metals. *Phys. Rev. B* **1993**, *48*, 13115−13118.
(22) Kresse, G.; Furthmüller, J. Efficient iterative schemes for ab initio total-energy calculations using a plane-wave basis set. *Phys. Rev. B* **1996**, *54*, 11169−11186.
(23) Perdew, J. P.; Burke, K.; Ernzerhof, M. Generalized gradient approximation made simple. *Phys. Rev. Lett.* **1996**, *77*, 3865−3868.
(24) Dion, M.; Rydberg, H.; Schroder, E.; Langreth, D. C.; Lundqvist, B. I. Van der Waals density functional for general geometries. *Phys. Rev. Lett.* **2004**, *92*, No. 246401.
(25) Blöchl, P. E. Projector augmented-wave method. *Phys. Rev. B* **1994**, *50*, 17953−17979.
(26) Kresse, G.; Joubert, D. From ultra-soft pseudopotentials to the projector augmented-wave method. *Phys. Rev. B* **1999**, *59*, 1758−1775.
(27) Troullier, N.; Martins, J. L. Efficient pseudopotentials for plane-wave calculations. *Phys. Rev. B* **1991**, *43*, 1993−2006.
(28) Weser, M.; Voloshina, E. N.; Horn, K.; Dedkov, Y. S. Electronic structure and magnetic properties of the graphene/Fe/Ni(111) intercalation-like system. *Phys. Chem. Chem. Phys.* **2011**, *13*, 7534−7539.
(29) Carra, P.; Thole, B. T.; Altarelli, M.; Wang, X. X-ray circular dichroism and local magnetic fields. *Phys. Rev. Lett.* **1993**, *70*, 694.
(30) Esquinazi, P.; Spemann, D.; Hohne, R. Induced magnetic ordering by proton irradiation in graphite. *Phys Rev. Lett.* **2003**, No. 227201.
(31) Xue, Y.; Wu, B.; Guo, Y.; Huang, L.; Jiang, L.; et al. Synthesis of large-area, few-layer graphene on iron foil by chemical vapor deposition. *Nano Res.* **2011**, *4*, 1208−1214.

DOI: 10.1021/acs.jpcc.9b05886
J. Phys. Chem. C 2019, 123, 26870−26876

(32) Li, X.; Cai, W.; An, J.; Kim, S.; Nah, J.; et al. Large-area synthesis of high-quality and uniform graphene films on copper foils. *Science* **2009**, *324*, 1312−1314.
(33) Kim, K. S.; Zhao, Y.; Jang, H.; Lee, S. Y.; Kim, J. M.; et al. Large-scale pattern growth of graphene films for stretchable transparent electrodes. *Nature* **2009**, *457*, 706−710.
(34) Chen, X.; Zhang, L.; Chen, S. Large area CVD growth of graphene. *Synth. Met.* **2015**, *210*, 95−108.
(35) Monkhorst, H. J.; Pack, J. D. Special points for Brillouin-zone integrations. *Phys. Rev. B* **1976**, *13*, 5188−5192.

DOI: 10.1021/acs.jpcc.9b05886
J. Phys. Chem. C 2019, 123, 26870−26876